PCCP

Accepted Manuscript

ROYAL SOCIETY OF CHEMISTRY

www.rsc.org/pccp

Journal Name

RSCPublishing

ARTICLE

Intense NIR emissions at 0.8 μm, 1.47 μm, and 1.53 μm from colloidal $LiYbF_4$:Ln^{3+} (Ln=Tm^{3+} and Er^{3+}) nanocrystals

Cite this: DOI: 10.1039/xoxxoooooox

Received ooth January 2012,
Accepted ooth January 2012

DOI: 10.1039/xoxxoooooox

www.rsc.org/

Shyam Sarkar,[a] Venkata N. K. B, Adusumalli, [a] Venkataramanan Mahalingam*[a] and John A Capobianco*[b]

We report on the synthesis of diamond shaped Ln^{3+}-doped $LiYbF_4$ (Ln=Tm and Er) nanocrystals with flat edges *via* the thermal decomposition method. Strong near-infrared emissions at 0.8 μm, 1.47 μm and 1.53 μm are observed from colloidal dispersions of Tm^{3+}-doped and Er^{3+}-doped $LiYbF_4$ nanocrystals, respectively under 0.98 μm diode laser excitation. The NIR emission intensities for Tm^{3+}-doped and Er^{3+}-doped $LiYbF_4$ nanocrystals are comparable with those of the sodium counterpart $NaYbF_4$ suggesting that $LiYbF_4$ is also an excellent host matrix for lanthanide ions to obtain strong NIR emissions in colloidal solutions of $LiYbF_4$ (Tm^{3+} or Er^{3+})nanocrystals.

1. Introduction

Upconverting nanomaterials which are able to convert lower energy radiation (near-infrared) to higher energy radiation (ultraviolet (UV) or visible) by absorbing one or more low energy photons are getting much attention recently owing to their potential use in a wide range of applications from optoelectronic devices to bioimaging.[1-15] The upconversion (UC) process is largely exhibited by lanthanide (Ln^{3+}) ions and generally occurs by three different mechanisms; energy transfer upconversion (ETU), excited state absorption (ESA) and photon avalanche (PA).[16-18] Among these mechanisms, ETU is predominantly observed in colloidal nanocrystals particularly in Yb^{3+} ions co-doped materials. Due to higher absorption coefficient of the Yb^{3+} ion compared to other Ln^{3+} ions, it is used as a sensitizer. Moreover, excitation wavelength of the laser diode (0.98 μm) may be used to excite the Yb^{3+} ions.[19,20] Among the available matrices for Ln^{3+} ions, fluorides are considered as ideal hosts due to their low phonon energy which reduces the nonradiative relaxations.[21-29]

There are several reports on upconverting Ln^{3+}-doped fluoride nanoparticles. One of the major interests of UC nanomaterials is in bioimaging since excitation at 0.98 μm allows deeper penetration of light in tissues, reduces auto-fluorescence and increases image contrast.[30-32] Particularly interesting are materials where the emission peaks are also in the NIR region. A number of reports can be found on NIR to NIR upconversion emission. For example, Prasad's group have shown NIR to NIR upconversion emission from ultrasmall Yb^{3+}/Tm^{3+}-doped $NaYF_4$ nanocrystals. By increasing the Yb^{3+} ions concentration from 20 to 100% a great enhancement (43 times) of NIR to NIR UC emission was observed.[33] The same group have also shown NIR to NIR downconversion photoluminescence from core/shell $NaGdF_4$:Nd^{3+}/$NaGdF_4$ nanocrystals.[34] In another study, they have shown NIR upconversion emission from core/shell $NaYbF_4$/CaF_2 nanocrystals which was used in high contrast deep tissue bioimaging.[35] However, the majority of the above mentioned studies concentrate on the 0.8 μm emission from Tm^{3+} or Nd^{3+} ions. NIR emissions particularly near 1.5 μm (1.53 μm and 1.47 μm) are interesting for telecommunication applications. These emissions have been reported in solid state materials however, only few reports are available on colloidal systems. This is probably due to the efficient quenching of these emissions by nonradiative relaxations. For example, 1.47 μm Stokes emission of Tm^{3+} ions has been reported for LaF_3:Tm^{3+}/LaF_3 core-shell nanoparticles.[36] We have reported similar ~1.46 μm emission from Yb^{3+}/Tm^{3+} co-doped $LiYF_4$ nanocrystals under 0.98 μm laser excitation.[37] However, to produce dispersible nanocrystals exhibiting strong NIR emissions at wavelengths above 0.8 μm remains a challenge. The advantage of colloidal nanocrystals would be the uniform coating over any surfaces and facile integration into thin film devices.

In this article, we report the synthesis of colloidal Ln^{3+}-doped $LiYbF_4$ nanocrystals (Ln=Tm^{3+} and Er^{3+}) stabilized by oleate ligands and produced *via* the thermal decomposition method (see experimental section for details). NIR (0.98 μm) to NIR (0.8 μm) emission *via* upconversion process was achieved by doping Tm^{3+} ions in the host matrix, $LiYbF_4$. Moreover, Tm^{3+}-doped and Er^{3+}-doped $LiYbF_4$ nanocrystals show strong 1.46 μm and 1.53 μm Stokes emissions *via* upconversion

respectively, which are important wavelengths for application in telecommunication.

2. Experimental

2.1 Materials and methods

All the chemicals used in this work, thulium oxide (Tm_2O_3, 99.99%), erbium oxide (Er_2O_3, 99.99%), ytterbium oxide (Yb_2O_3, 99.99%), trifluoroacetic acid (CF_3COOH, 99%), oleic acid (90%), 1-octadecene (90%) and lithium trifluoroacetate (CF_3COOLi, 99.99%), sodium trifluoroacetate (CF_3COONa, 99.99%), absolute ethanol were purchased from Sigma Aldrich. All the materials were used without further purification.

2.2 Synthesis of nanocrystals

Ln^{3+}-doped $LiYbF_4$ nanocrystals were prepared *via* the thermal decomposition method using oleic acid as capping agent and 1-octadecene as high boiling point solvent. Briefly, lanthanide trifluoroacetates were first prepared by refluxing stoichiometric amounts of corresponding lanthanide oxides with 1:1 trifluoroacetic acid and water at 85^0C and then evaporated at 65^0C to dryness. CF_3COOLi, oleic acid (20 mL) and 1-octadecene (20 mL) were added to dried precursors and the resulting mixture was heated to 120°C under vacuum. After 15 minutes, the temperature of the mixture was raised to 310°C under an argon flow for 1 h. The mixture was cooled to room temperature and the nanocrystals were precipitated with absolute ethanol. The nanocrystals were separated by centrifugation and further purified by dispersing them in hexane followed by precipitation again with absolute ethanol. A 1 wt% colloidal dispersion was prepared by dispersing approximately 100 mg of the nanocrystals in 10 mL of toluene.

2.3. Characterization techniques

Powder X-ray diffraction (PXRD):
Analysis of the phase of the as prepared Ln^{3+}-doped $LiYbF_4$ (Ln=Tm or Er) nanocrystals was carried out by powder X-ray diffraction (XRD) measurements, using a Rigaku-smartlab diffractometer with Cu Kα operating at 200 kV and 45mA at a scanning rate of 1º min^{-1} in the 2θ range from 15º to 90º. The samples were spread evenly on a quartz slide.
Transmission electron microscopy (TEM):
The morphology of the nanocrystals were characterized by transmission electron microscopy (TEM), using a FEI (Czech Republic), FP5018/40 TECHNAI G^2 SPIRIT BioTWIN transmission electron microscope operated at 120 keV. Prior to analysis, a 10 mg sample was dispersed in 10 ml of toluene to make a 0.1 wt% solution. A drop of the toluene dispersion was evaporated on a carbon coated 300 mesh copper grid.
Scanning electron microscopy (SEM):
Scanning electron microscopy (SEM) images were taken using a ZEISS (SUPRA) instrument. Prior to loading of the samples into the chamber, they were coated with a thin film of gold-palladium in order to avoid charging effects.
Fourier transform infrared (FTIR) spectroscopy:
The FTIR spectra were recorded using a Perkin Elmer Spectrum RX1 spectrophotometer with the KBr disk technique in the range of 400-4000 cm^{-1}. The FTIR spectra of the samples was recorded using 10 mg of the samples mixed with 200 mg of KBr to produce the pellets.
Luminescence studies:
The upconversion emission (UC) spectra were obtained by exciting a 1 wt (%) solution (nanocrystals dispersed in toluene) using a 0.98 µm diode laser (RGB Lase LLC), which was coupled with a fibre with a core diameter of 100 µm,. The output signal was measured with a Jobin Yvon Fluoromax-4 spectrometer. The 1.47 µm emissions were collected using a Jobin Yvon Fluorolog system under 0.98 µm CW diode laser excitation and the signal was detected using a NIR PMT module detector (HAMAMATSU, H10330A series).

3. Results and discussion

Powder X-ray diffraction (XRD) pattern of the 1 mol(%) Tm^{3+}-doped $LiYbF_4$ nanocrystals and the standard pattern for $LiYbF_4$ crystals are shown in Fig. 1. The XRD pattern of $LiYbF_4$ nanocrystals is in agreement with the standard pattern of tetragonal $LiYbF_4$ crystals (ICSD PDF Card No.-01-071-1211) suggesting the formation of pure tetragonal phase nanocrystals. Similarly, the XRD patterns of 2 mol(%) Er^{3+}-doped $LiYbF_4$ nanocrystals matches with that of standard pattern of $LiYbF_4$ crystals (see Fig. S1, ESI†).

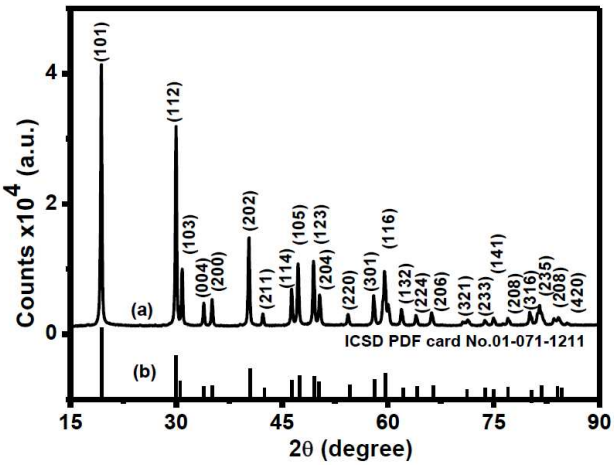

Fig. 1 XRD patterns of (a) 1 mol(%) Tm^{3+}-doped $LiYbF_4$ nanocrystals and (b) standard bulk $LiYbF_4$ (ICSD PDF Card No. 01-071-1211).

The $LiYbF_4$ nanocrystals crystallize in tetragonal phase with $I4_1/a$ space group. The lattice constants of tetragonal $LiYbF_4$ nanocrystals were found to be a=b=5.1005Å, c=10.5564Å. These values match well with the standard values a=b=5.1335Å, c=10.5880Å for bulk $LiYbF_4$. The slight increase in the 'a' and 'b' values could be due to the larger ionic radii of the dopant ions, Tm^{3+} (r=0.994Å) compared to the Yb^{3+} ions (r=0.985Å). The structure of the tetragonal unit cell of $LiYbF_4$ is shown in Fig. 2, which is drawn using the Visualization for Electronic and Structural Analysis (VESTA)

program using the lattice parameters obtained from the XRD diffraction measurements and the atomic coordinates from the literature.[38] Coordination of Yb^{3+} ions with F^- ions are also shown in the unit cell structure. The Yb^{3+} ions are surrounded by eight fluoride ions that form the edges of a slightly distorted dodecahedron.[39,40]

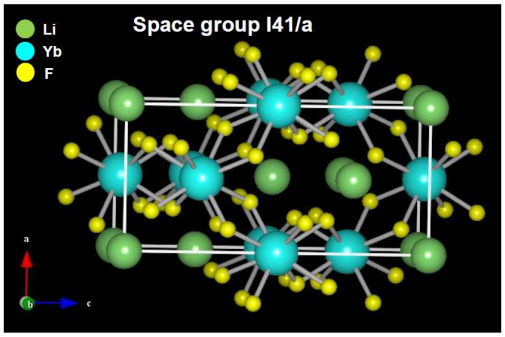

Fig. 2 Schematic representation of the tetragonal unit cell structure of $LiYbF_4$ nanocrystals. The coordination of Yb^{3+} ions is also shown.

Morphological analyses of the as synthesized Tm^{3+}-doped $LiYbF_4$ nanocrystals have been performed using high resolution transmission electron microscopy (HRTEM) and SEM. The HRTEM image of the Tm^{3+}-doped $LiYbF_4$ nanocrystals are shown in Fig. 3 and in Fig. S2. It is important to note that the shape of the 1 mol(%) Tm^{3+}-doped $LiYbF_4$ nanocrystals show slightly flattened edges of the perfect diamond with an average aspect ratio (length/breadth) of 1.4 as shown in the histogram (Fig. 3B). We emphasize that in TEM analysis we observed few nanocrystals with larger size (~80 nm) with similar morphology. However, the number of larger particles is very low. The observed shape is slightly different from that reported for $LiYF_4$ nanocrystals by Mahalingam *et al.*[37]

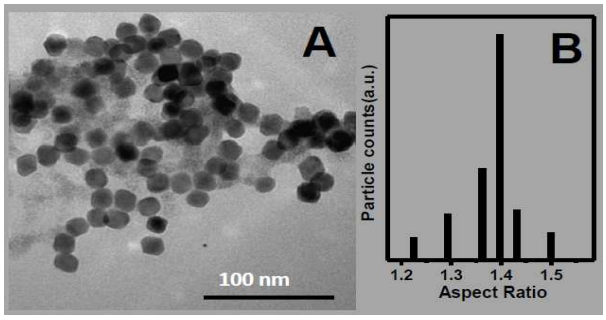

Fig 3 (A) TEM image of Tm^{3+}-doped $LiYbF_4$ nanocrystals, and (B) particle size (aspect ratio) distribution.

We postulate that this could be due to the difference in the ionic radii of the Ln^{3+} ions. In the case of Yb^{3+}/Tm^{3+}-doped $LiYF_4$ nanocrystals, the ionic radius of the Y^{3+} ion is 1.019 Å, which is larger than the ionic radii of the dopant ions Tm^{3+}(r=0.994 Å) and Yb^{3+} (r=0.985 Å). Whereas, in the case of $LiYbF_4$ the ionic size of Yb^{3+} is smaller than the Tm^{3+} (r=0.994 Å) or Er^{3+} (r=1.004 Å) ions. This causes a slight expansion of the lattice that is reflected in the lattice parameters (*vide supra*) and such expansion may result in a slight distortion at the tip of the diamond, as they possess higher surface energy. The observed, slightly flattened diamond shape morphology of the nanocrystals is further supported by scanning electron microscopy (SEM) measurement. The SEM image of the 1 mol(%) Tm^{3+}-doped $LiYbF_4$ nanocrystals is shown in Fig. S3 (see ESI†).

The oleate capping of the surface of the nanocrystals is confirmed by Fourier Transform Infra-red (FTIR) measurements. The FTIR spectra of the oleate capped Tm^{3+}-doped $LiYbF_4$ nanocrystals and pure oleic acid are shown in Fig. S4 (see ESI†). It is clear from the spectra that the peak at 1715 cm^{-1} observed in free oleic acid shifts to the lower wavenumber (1545 cm^{-1}) for the oleate capped nanocrystals indicating that $-COO^-$ groups of oleic acid are bound to the surface of the nanocrystals.[41] The long aliphatic chain of oleic acid renders the nanocrystals dispersible in hydrophobic solvents like hexane, toluene, etc.

The upconversion (UC) emission spectrum of the 1wt% toluene dispersion of the $LiYbF_4$:Tm^{3+}(1%) nanocrystals under 0.98 µm CW diode laser excitation is shown in Fig. 4. A strong emission peak around 0.8 µm corresponding to the $^3H_4 \rightarrow {}^3H_6$ transition is clearly visible in the UC emission spectrum. Along with the 0.8 µm peak three peaks at 0.478 µm, 0.65 µm and 0.7 µm are observed whose emission intensities are relatively weak in comparison to the 0.8 µm peak emission intensity. The corresponding peak assignments are shown in the Fig. 4. This observation is different from that of the Yb^{3+}/Tm^{3+}-doped $LiYF_4$ nanocrystals.[10] Generally, in Yb^{3+}/Tm^{3+} co-doped systems such as, $LiYF_4$:Yb^{3+}/Tm^{3+} and $NaYF_4$:Yb^{3+}/Tm^{3+} the blue emission is quite intense and nearly the same as the NIR emission. A comparison of the UC emission spectra (shown in Fig. 5) of Yb^{3+}(20%)/Tm^{3+}(1%)-doped $LiYF_4$ and Tm^{3+}(1%)-doped $LiYbF_4$ nanocrystals prepared and measured under identical conditions show a high NIR to blue emission intensity ratio for the Tm^{3+}-doped $LiYbF_4$ nanocrystals.

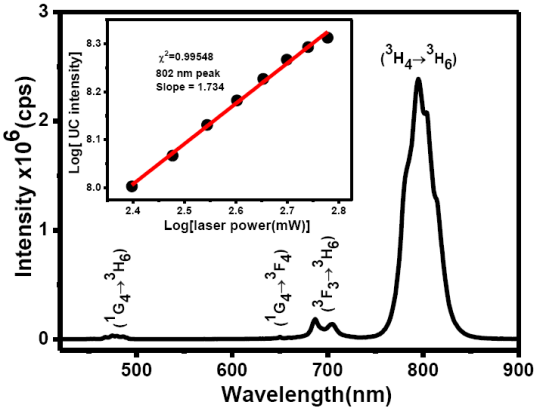

Fig. 4 The UC emission spectrum of 1 mol(%) Tm^{3+}-doped $LiYbF_4$ nanocrystals under 0.98 µm excitation. Inset shows logarithmic plot of UC emission intensity versus laser power for the 0.8 µm peak.

To understand the reason for the observed differences and to ascertain the number of photons involved in the UC process we performed power dependent UC emission studies. The UC emission intensity(I) is proportional to the laser power (P), raised to the n where n is the number of incident photons

[$I \propto P^n$]. From this equation, n can be determined by plotting Ln(I) vs. Ln(P). For the NIR emission (0.8 μm) of Tm^{3+}-doped $LiYbF_4$ nanocrystals (Fig. 4 inset) the calculated value of n is found to be 1.73 which, implies the involvement of two photons in the UC processes. The proposed energy transfer mechanism is discussed below.

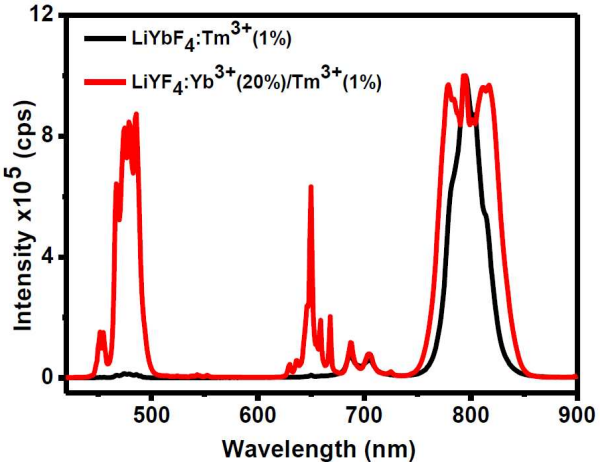

Fig. 5 The upconversion emission spectra of $LiYbF_4$:Yb^{3+}(20%)/Tm^{3+}(1%) (red trace) and $LiYbF_4$:Tm^{3+}(1%) (black trace) nanocrystal under 0.98 μm excitation with a laser power density 70W/Cm^2.

It is quite likely that the selective quenching of the blue emission or visible emissions might be due to back transfer of the energy to the Yb^{3+} ions. However, if back energy transfer alone is occurring then it should affect the 800 nm emission more compared to other emissions as the $^3H_4$ level is closer in energy. So we believe there is additional cross relaxations (CR) occurring along with the back energy transfer. This alone cannot explain the observed results. We propose the following two CR mechanisms occurring in the materials studied; [$^1G_4$, $^3H_6 \rightarrow {}^3F_2, {}^3F_4$] and [$^1G_4$, $^3H_6 \rightarrow {}^3H_4$, $^3H_5$]. These CR processes lead to the population of the $^3F_{2,4}$, and $^3H_{4,5}$ levels. Thus the emission intensities of the transition (700 nm and 800 nm) originating from these levels are not affected to a large extent whereas the transitions originating from $^1G_4$ level are affected.

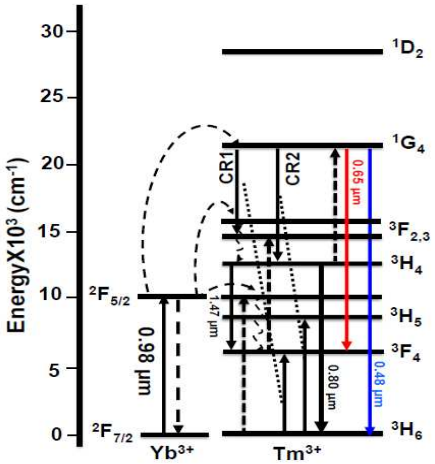

Fig. 6 Schematic energy level diagram with predicted energy transfer mechanism between Yb^{3+} and Tm^{3+} ions in $LiYbF_4$ nanocrystals. The two cross relaxations processes are denoted as CR1 and CR2.

Similar CR processes have been reported for Tm^{3+}-doped tellurite glasses.[42] A schematic of the possible energy transfer mechanism between Yb^{3+} and Tm^{3+} ions along with CR processes are shown in Fig. 6.

To understand the influence of Tm^{3+} ions concentration on the UC emission intensity of the $LiYbF_4$ nanocrystals and to determine the optimal concentration of Tm^{3+} ions in $LiYbF_4$ matrix, a series of samples with 0.5, 0.75, 1.0 and 1.5 mol% Tm^{3+} ions were prepared. As shown in Fig. 7 the intensity of the NIR emission (0.8 μm) is highest for 1.0% Tm^{3+}-doped $LiYbF_4$ nanocrystals. A plot of the integrated area of UC emission spectra as a function of Tm^{3+} ions concentration are shown in the inset of Fig. 7. It is also evident from the spectra that the change in UC emission intensity with concentration of Tm^{3+} ions is not the same for the emission peaks at 0.478 μm, 0.65 μm and 0.8 μm.

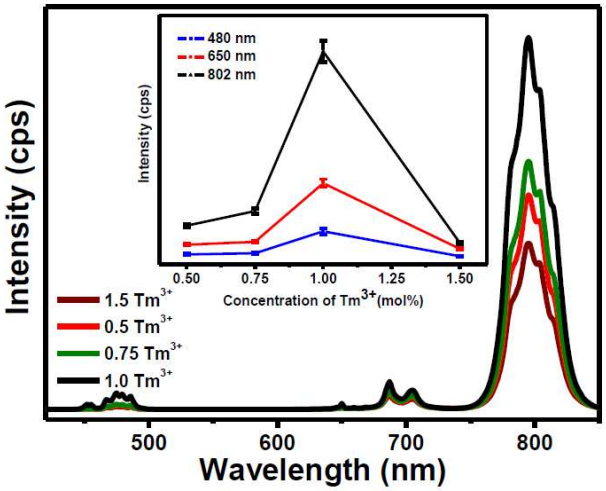

Fig. 7 The upconversion emission spectra of Tm^{3+}-doped $LiYbF_4$ nanocrystal as a function of Tm^{3+} concentration under 0.98 μm diode laser with a laser power 70W/cm^2. Inset shows the UC emission intensity as a function of Tm^{3+} ions concentration.

We have extended the study to Er^{3+}-doped $LiYbF_4$ nanocrystals. The UC emission spectrum from a colloidal dispersion of 2 mol(%) Er^{3+}-doped $LiYbF_4$ nanocrystals is shown in Fig. 8. The UC emission spectrum shows two peaks at 0.52 and 0.54 μm, which are assigned to the $^2H_{11/2} \rightarrow {}^4I_{15/2}$ and $^4S_{3/2} \rightarrow {}^4I_{15/2}$ transitions, respectively. It is interesting to note that both transitions show approximately equal intensity, though the energy difference between the two levels is only 760 cm^{-1} and can easily be matched with few phonon vibrations. We assume that the same intensity of these two peaks may be due to thermal equilibration of the population leading to equal distribution. However, the green emission peaks are less intense compared to red peak at 0.65 μm, which corresponds to $^4F_{9/2} \rightarrow {}^4I_{15/2}$ transitions. To ascertain that this is not due to weak green UC emission from $LiYbF_4$:Er^{3+}(2%) nanocrystals we have compared UC emission spectra of both Yb^{3+}(20%)/Er^{3+}(2%)-doped $LiYF_4$ and Er^{3+}(2%)-doped $LiYbF_4$ nanocrystals under identical condition (Fig. S5, see ESI†). From the spectra it is clear that UC emission intensity of the green peak is lower than the red emission in $LiYbF_4$ compared to that of Y^{3+} counterpart.

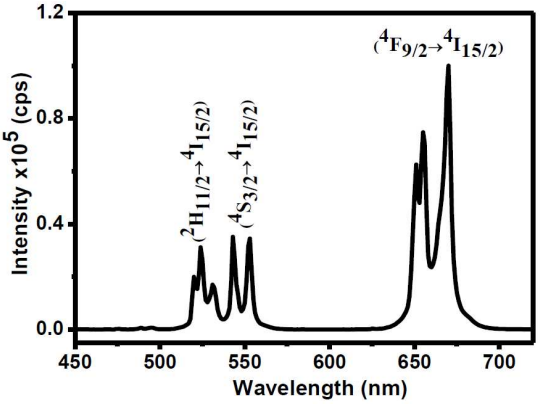

Fig. 8 Upconversion emission spectrum of 2 mol(%) Er^{3+}-doped $LiYbF_4$ nanocrystals upon 0.98 μm laser excitation.

[43] It is already established that, at high levels of doping of donor Yb^{3+} ions, some of those Yb^{3+} ions act as quenchers which induce a quenching effect via $Er^{3+}\rightarrow Yb^{3+}$ back transfer.[43,44] This is evident in the UC of the Er^{3+}(2%)-doped $LiYbF_4$ nanocrystals where the overall UC emission intensity is lower than that of Yb^{3+}(20%)/Er^{3+}(2%)-doped $LiYF_4$ nanocrystals (see Fig. S5, ESI†). Furthermore, the lifetime of Er^{3+} ions in the Er^{3+}(2%)-doped $LiYbF_4$ nanocrystals is lower than that of the Yb^{3+}(20%)/Er^{3+}(2%)-doped $LiYF_4$ nanocrystals which also suggest the back transfer. The corresponding decay curves were measured under 0.488 μm direct excitation of Er^{3+} ions (see Fig. S6, ESI†). However, if back energy transfer alone occurs then it should be more probable from red emitting state ($^4F_{9/2}$) as this level is closer in energy with respect to excited Yb^{3+} level ($^2F_{5/2}$) in comparison to the green emitting levels ($^2H_{11/2}$ and $^4S_{3/2}$). Moreover, the intensity of the red emission is not affected to any great extent. As back energy transfer is quite probable, there must be additional feedback system(s) operating in the material preferentially populating the red emitting level. Thus, we proposed the cross-relaxation mechanism occurring between Yb^{3+} and Er^{3+} ions, which is quite possible since there is a higher concentration of Yb^{3+} ions in the matrix. The possible energy transfer mechanisms between Yb^{3+} and Er^{3+} ions are shown in Fig. S7 (see ESI†). In this mechanism, the Yb^{3+} ions act as sensitizers and Er^{3+} ions as activator in the upconversion process. Under 0.98 μm laser excitation electrons from the ground state, $^2F_{7/2}$, of Yb^{3+} are promoted to the excited state, $^2F_{5/2}$, followed by the transfer of energy from the $^2F_{5/2}$ level of Yb^{3+} to the $^4I_{11/2}$ level of Er^{3+}. Through a second energy transfer from the $^2F_{5/2}$ level of Yb^{3+} to the $^4I_{11/2}$ level of Er^{3+} the electrons are promoted to the $^4F_{7/2}$ level (Er^{3+}). The electrons in the excited state decay non-radiatively to $^2H_{11/2}$, $^4S_{3/2}$ and $^4F_{9/2}$ energy levels and then radiatively decay to the ground state ($^4I_{15/2}$) of Er^{3+} ions giving rise to green and red emissions, respectively. Along with these processes the suggested cross relaxations and the back energy transfer occur to selectively depolulate the green emitting levels (*vide supra*)

The optical study of Ln^{3+}-doped $LiYbF_4$ (Ln=Tm^{3+} or Er^{3+}) nanocrystals was extended to the telecommunication window (1.46-1.54 μm). Interestingly, under 0.98 μm laser excitation a Stokes emission peak around 1.47 μm is observed from the 1 wt(%) colloidal Tm^{3+}-doped $LiYbF_4$ nanocrystals. The 1.47 μm emission is assigned to $^3H_4\rightarrow{}^3F_4$ transitions, which is a very important wavelength as it falls in the S-band (1.46-1.54 μm) region of optical telecommunication. Similarly, an intense near-infrared luminescence peak close to 1.53 μm (corresponding to $^4I_{13/2}\rightarrow{}^4I_{15/2}$ transition) is observed from the 2 mol (%) Er^{3+}-doped $LiYbF_4$ nanocrystals. The NIR emission spectra of Tm^{3+}-doped and Er^{3+}-doped $LiYbF_4$ nanocrystals are shown in Fig. 9A and 9B, respectively. It is reasonable to assume that the 1.47 μm emission from Tm^{3+} ions occurs *via* a two photon process as the emitting level ($^3H_4$) is higher in energy compared to $^2F_{5/2}$ level of Yb^{3+} ions.[37] Whereas, the NIR emission observed at the 1.53 μm for Er^{3+} ions due to $^4I_{13/2}\rightarrow{}^4I_{15/2}$ transition may occur *via* a single photon process. The logarithmic plots of intensity vs. laser power for Tm^{3+}-doped (1.47 μm) and Er^{3+}-doped (1.53 μm) $LiYbF_4$ nanocrystals are shown in Fig. S8 and Fig. S9, respectively, (see ESI†). Linear fitting of these two curves led to the slope values 1.37 and 0.98 respectively for 1.47 μm (Tm^{3+}) and 1.53 μm (Er^{3+}) peaks.

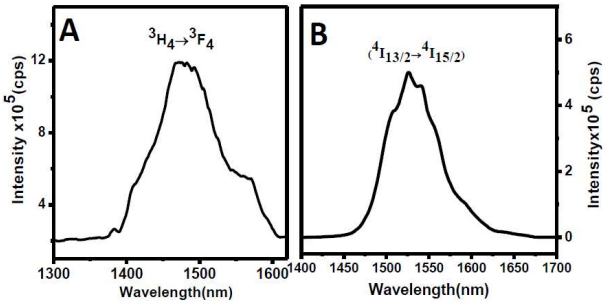

Fig. 9 The NIR emission spectra of (A) 1 mol(%) Tm^{3+}-doped and (B) 2 mol(%) Er^{3+}-doped $LiYbF_4$ nanocrystals upon 0.98 μm laser excitation.

The Ln^{3+}-doped $NaYbF_4$ (Ln=Tm and Er) nanocrystals are prepared under identical condition to understand how strong are the NIR emissions from Ln^{3+}-doped $LiYbF_4$ nanocrystals compared to the host $NaYbF_4$. The comparison of NIR emission spectra of Ln^{3+}-doped $NaYbF_4$ and $LiYbF_4$ nanocrystals are shown in Fig. 10. The UC spectra shown in Fig. 10 (A, B) indicate that the NIR emission intensities for Tm^{3+}-doped and Er^{3+}-doped $LiYbF_4$ nanocrystals are almost comparable with that of $NaYbF_4$ counterpart. The above result reveals that $LiYbF_4$ is an excellent host matrix for lanthanide ions to obtain strong NIR emissions in colloidal nanocrystals.

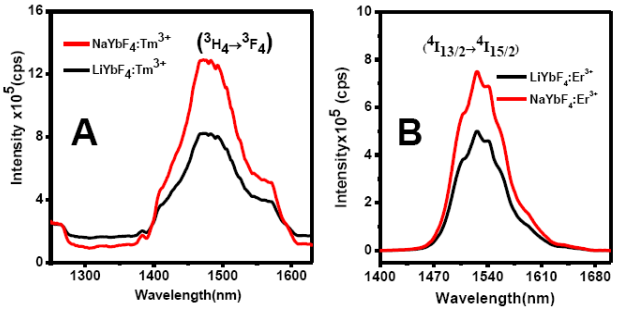

Fig. 10 Comparison of the NIR emission spectra of (A) $NaYbF_4$:Tm^{3+} vs. $LiYbF_4$:Tm^{3+} and (B) $NaYbF_4$:Er^{3+} vs. $LiYbF_4$:Er^{3+} obtained via 0.98 μm laser excitation.

4. Conclusions

In summary, we have synthesized Ln^{3+}-doped $LiYbF_4$ (Ln=Tm^{3+} and Er^{3+}) nanocrystals *via* the thermal decomposition method. The nanocrystals are diamond shaped and slightly flattened at the edges. Strong NIR (0.8 μm) emission compared to visible emissions was observed from the colloidal dispersion of the 1 mol(%) Tm^{3+}-doped $LiYbF_4$ nanocrystals under excitation at 0.98 μm diode laser. We have proposed a cross relaxation mechanism for the selective quenching of the visible emission over the NIR emission. Moreover, Stokes emissions *via* upconversion process around 1.47 μm and 1.53 μm were observed respectively from Tm^{3+}-doped and Er^{3+}-doped $LiYbF_4$ nanocrystals which can find applications in telecommunication in addition to their use in bioimaging applications.

Acknowledgements

VM thanks Council of Scientific and Industrial Research (CSIR), India and IISER-Kolkata for financial support. SS thanks to UGC, India for his fellowship. JAC is a Concordia University Research Chair in Nanoscience and is grateful to Concordia University and NSERC for financial support of his research.

Notes and references

[a] Department of Chemical Sciences, Indian Institute of Science Education and Research (IISER), Kolkata, Mohanpur, West Bengal 741252, India. Fax: 91-33-25873020; Tel: +91(0)9007603474
E-mail: mvenkataramanan@yahoo.com
[b] Department of Chemistry and Biochemistry and Centre for NanoScience Research, Concordia University, Montreal, Quebec, H4B 1R6, Canada
E-mail: john.capobianco@concordia.ca

†Electronic Supplementary Information (ESI) available: [PXRD pattern, SEM image, FTIR spectra, UC emission spectra, lifetime decay curves and UC energy transfer mechanism]. See DOI: 10.1039/b000000x/

1 G. Blasse and B. C. Grabmaier, *Luminescent Materials*, Springer, Berlin, 1994.
2 J.-C. G. Bünzli *Chem. Rev*., 2010, **110**, 2729-2755.
3 C. G. Bünzli *Chem. Rev*., 2002, **102**, 1897-1928.
4 G. Ozen, O. Forte, and B. D. Bartolo, *Opt. Mater*., 2005, **27**, 1664-1671.
5 T. Yang, Y. Sun, Q. Liu, W. Feng, P. Yang, and F. Li, *Biomaterials*, 2012, **33**, 3733-3742.
6 D. Jaque, L. Martínez Maestro, B. del Rosal, P. Haro-Gonzalez, A. Benayas, J. L. Plaza, E. Martín Rodríguez and J. García Solé, *Nanoscale*, 2014, 6, 9494.
7 T. Cao, Y. Yang, Y. Gao, J. Zhou, Z. Li, and F. Li, *Biomaterials*, 2011, **32**, 2959-2968.
8 J. C. Boyer, F. Vetrone, L. A. Cuccia, J. A. Capobianco, *J. Am. Chem. Soc*. 2006, **128**, 7444-7445.
9 F. Wang, X. J. Xue, and X. Liu, *Angew. Chem. Int. Ed.,* 2008, **47**, 906-909.
10 F. Wang, Y. Han, C. S. Lim, Y. Lu, J. Wang, J. Xu, H. Chen, C. Zhang, M. Hong, and X. Liu, *Nature*, 2010, **463**, 1061-1065.
11 C. Li, and J. Lin, *J. Mater. Chem*., **2010**, 20, 6831-6847.
12 X. Zhang, P. Yang, C. Li, D. Wang, J. Xu, S. Gai, and J. Lin, *Chem. Commun*., 2011, **47**, 12143-12145.
13 T. He, W. Wei, L. Ma, R. Chen, S. Wu, H. Zhang, Y. Yang, J. Ma, L. Huang, G. G. Gurzadyan, and H. Sun, *Small,* 2012, **8**, 2163-2168.
14 A. Patra, S. Saha, M. A. R. C. Alencar, N. Rakov, and G. S. Miciel, *Chem. Phys. Lett*., 2005, **407**, 477-481.
15 A. Patra, C. S. Friend, R. Kapoor, P. N. Prasad, *J. Phys. Chem. B,* 2002, **106**, 1909-1912.
16 F. Auzel, *Chem. Rev*., 2004, **104**, 139-173.
17 S. Sivakumar, F. C. J. M. van Veggel, P. S. May, *J. Am. Chem. Soc.,* 2007, **129,** 620-625.
18 J. C. Boyer, N. J. J. Johnson, F. C. J. M. van Veggel, *Chem. Mater.,* 2009, **21**, 2010-2012.
19 M. Haase and H. Schäfer, *Angew. Chem. Int. Ed.,* 2011, **50***,* 5808-5829.
20 V. Mahalingam, R. Naccache, F. Vetrone, and J. A. Capobianco, *Chem. Commun*., 2011, **47,** 3481-3483.
21 G. Wang, Q. Peng and Y. Li, *J. Am. Chem Soc.*, 2009, **131**, 14200-14201.
22 O. Ehlert, R. Thomann, M. Darbandi and T. Nann, *ACS Nano*, 2008, **2**, 120-124.
23 C. Dong, and F. C. J. M. van Veggel, *ACS Nano,* 2009, **3,** 123-130.
24 S. Sarkar, C. Hazra and V. Mahalingam, *Chem Eur J.*, 2012, **18**, 7050-7055.
25 S. Sarkar, C. Hazra, M. Chatti, V. Sudarsan and V. Mahalingam, *RSC Adv*., 2012, **2**, 8269-8272.
26 S. Sarkar, B. Meeseragandla, C. Hazra and V. Mahalingam, *Adv. Mater.*, 2013, **25**,856-860.
27 S. Sarkar and V. Mahalingam, *CrystEngComm.*, 2013, **15**, 5750-5755.
30 D. K. Chatterjee,M. K. Gnanasammandhan, Y. Zhang, *Small,* 2010, **6**, 2781-2795.
31 F. Wang, D. Banerjee, Y. Liu, X. Chen, X. Liu, *Analyst*, 2010, **135**, 1839-1854
32 L. M. Maestro, J. E. Ramirez-Hernandez, N. Bogdan, J. A. Capobianco, F. Vetrone, J. García Solé, D. Jaque, *Nanoscale*, 2011, **4**, 298-302.
33 G. Chen, T. Y. Ohulchanskyy, R. Kumar, H. Ågren and P. N. Prasad, *ACS Nano*, 2010, **4**, 3163-3168.
34 G. Chen, T. Y. Ohulchanskyy, S. Liu, W. C. Law, F. Wu, M. T. Swihart, H. Agren and P. N. Prasad, *ACS Nano,* 2012, **6**, 2969-2977.
35 G. Chen, J. Shen, T. Y. Ohulchanskyy, N. J. Patel, A. Kutikov, Z. Li, J. Song, R. K. Pandey,H. Agren, P. N. Prasad and G. Han, *ACS Nano*, 2012, **6**, 8280-8287.
36 P. R. Diamente, M. Raudsepp and F. C. J. M. van Veggel, *Adv. Funct. Mater.*, 2007, **17**, 363-368.
37 V. Mahalingam, F. Vetrone, R. Naccache, A. Speghini and J. A. Capobianco, *Adv. Mater*., 2009, **21,** 4025-4028.
38 K. Momma and F. Izumi, *J. Appl. Crystallogr.,* 2008, **41**, 653-658.
39 H. D. Leebeeck, K. Binnemans and C. G. Walrand, *Journal of Alloys and Compounds*, 1999, **291**, 300-311.
40 A. Grzechnik, K. Friese, V. Dmitriev, H. P. Weber, J. Y. Gesland and W. A. Crichton, *J. Phys. Condens. Matter,* 2005, **17**, 763-770.
41 S. Sarkar, C. Hazra and V. Mahalingam, *Dalton Trans.,* 2013, **42**, 63-66.
42 B. Zhou, H. Lin, and E. Y.-B. Pun1, *Optics Express*, 2010, **18**, 18805.

43 F. Vetrone, J. C. Boyer, J. A. Capobianco, A. Speghini and M. Bettinelli, *J. Appl. Phys.*, 2004, **96**, 661-667.
44 F. Auzel, G. Baldacchini, L. Laversenne, and G. Boulon, *Opt. Mater.*, 2003, **24**, 103-109.

TOC figure